CrystEngComm

Accepted Manuscript

Cite this: DOI: 10.1039/c0xx00000x
www.rsc.org/xxxxxx
ARTICLE TYPE

Rare-earth doped LaF_3 hollow hexagonal nanoplates: hydrothermal synthesis and photoluminescence property

Dangli Gao,*[a] Dongping Tian,[a] Bo Chong,[a] Xiangyu Zhang,[b] Wei Gao[c]

Received (in XXX, XXX) Xth XXXXXXXXX 20XX, Accepted Xth XXXXXXXXX 20XX
DOI: 10.1039/b000000x

A facile hydrothermal route at designated pH values has been developed to synthesize a series of well-dispersed LaF_3 colloidal nanocrystals (NCs) with a rich variety of morphologies, including nanoparticles, hexagonal nanoplates and fullerene-like nanoparticles. X-ray diffraction, scanning electron microscopy, transmission electron microscopy, high-resolution transmission electron microscopy, Fourier transform infrared spectroscopy, and photoluminescence spectra were used to characterize the samples. It is found that the formation of monodispersed fluoride NCs not only closely correlates with the pH values of the mother solutions, but also depends on the basicity of the base employed adjusting pH value. The strong alkaline solution in the absence of any organic additive in this system was found to be a prerequisite for producing hexagonal fullerene-like LaF_3 nanodisks. A mechanism for the formation of the fullerene-like LaF_3 via the local Ostwald ripening has been proposed based on observations of time-dependent experiments. The multicolor upconversion (UC) emission was successfully realized in a series of Yb^{3+}/Er^{3+} doped LaF_3 NCs by excitation in the near-infrared region. The UC emission ratios of red to green for a series of LaF_3 NCs can be tuned by adjusting the pH values of the mother liquids and an UC mechanism activated by the high energy phonons inherent in the hollow LaF_3 nanoplates is proposed. It is expected that these rare-earth fluoride NCs might have potential in applications for photocatalysis, biolabelling and drug-delivery.

Introduction

LaF_3 nanocrystals (NCs) are one of the most efficient host materials for upconversion (UC) processes, which can be applied in the fields of lighting, display technology and biolabels. So the synthesis of LaF_3 nanomaterials has attracted considerable interest and various methods have been developed recently.[1–3] To the best of our knowledge, most of the available synthetic approaches involving modified precipitation, polyol, and hydrothermal methods are based on the liquid precipitation reaction between rare-earth (RE) nitrates/chlorides and HF/NaF/NH_4F. But the LaF_3 NCs obtained by these methods were generally spherical or irregular in shape, because of the rapid nucleation process involved. So it still remains a challenge to find a suitable reaction system for growing high-quality LaF_3 NCs in terms of monodisperse, well-shaped, and single-crystalline NCs. Yan and co-workers first reported the synthesis of LaF_3 triangular nanoplates via a single source precursor $La(CF_3COO)_3$ route, but these nanoplates are inactive in UC luminescence.[4] Similar methods were then employed by several groups to synthesize $NaYF_4$ crystals.[5–7] Unfortunately, these methods were based on the thermo-decomposition of RE trifluoroacetates [$RE(TFA)_3$, RE = La, Y, Yb, Er and Tm] at high temperature in organic solvents, which need severe experimental conditions (300 ^{o}C, waterless, oxygen-free and inert gas protection). Therefore, it still remains a challenge to identify a suitable reaction system for growing high-quality RE doped LaF_3 NCs with novel structure and UC luminescence. The keys to a successful synthesis are to select suitable precursors, to control the coordinating behavior of the ligand and the growth rates.[8–13]

Synthesis of monodispersed hollow spheres is currently attracting continuous interest because these hollow spheres have potential applications in catalysis, photonic crystal, chromatography, protection of biologically active agents, fillers (or pigments, coatings), and dye sensitized solar cells.[14–18] In particular, the hollow spheres composed of RE doped nanoparticles are of interest recently not only because of their diverse properties, such as high quantum yield, low photobleaching, narrow emission band, and long luminescent lifetime,[19] as compared with conventional luminescent materials, but also because these luminescent hollow spheres could be used as carrier of targeted drugs for bioapplications.[20] For instance, Shan *et al*. fabricated hollow $NaYF_4$ NCs via the co-thermolysis of a mixture of trifluoroacetate precursors in trioctylphosphine oxide by Kirkendall effect.[21] Jia *et al.* prepared well-shaped Y_2O_3:Eu hollow microspheres via a urea-based homogeneous precipitation technique in the presence of colloidal carbon spheres as hard templates followed by a subsequent heat treatment process.[22] Zhang *et al*. obtained RE hollow cubic phase $NaYF_4$ nanoparticles by a controlled ion exchange process from cubic phase Y_2O_3 nanospheres.[23] These preparation processes are attractive, however, some evident defects, such as cumbersome and time-consuming physical and chemical processes in templates is insurmountable, whereas Kirkendall effect and Ostwald ripening techniques are primarily limited to specific materials such as metals, metal oxides, and chalcogenides (including Au, Ag, platinum cobalt oxides).[24] Recently, Chen *et al*. described the fabrication of EuF_3 and SmF_3 hollow sub-microcrystals by hydrothermal route in the presence of ethylenediaminetetraacetic acid (EDTA).[25,26] PrF_3 hollow nanoparticles were synthesized under the microwave-assisted heating hydrothermal conditions by Ma *et al*..[27] These nano/micro particles are well characterized as the paper brings some news in the synthetic concept in nanoparticle chemistry. So the discovery and exploitation of a facile and green universal method to prepare high quality hollow RE doped NCs is urgently required. To the best of our knowledge, there have been no reports on uniform RE doped LaF_3 hexagonal hollow nanoplates (fullerene-like nanoparticles) with bright UC luminescence. Moreover, few studies have focused on how the shapes and structures of RE doped LaF_3 nanomaterials, that is desirable for biolabels and drug-delivery applications, affect on luminescence and electronic transition properties.

In this paper, a simple hydrothermal approach in the absence of any organic additive at the designated pH value and reactive temperature, was proposed to synthesize monodispersed RE doped LaF_3 nanoparticles. By controlling pH in solution, LaF_3 spherical nanoparticles, hexagonal nanoplates and fullerene-like nanoparticles could be selectively synthesized. Furthermore, we systematically discuss the growth process of a series of LaF_3 NCs and UC luminescence properties adjusted by pH values. These RE doped LaF_3 NCs show great potential applications as bio-probes and drug-delivery.

Experimental

Chemicals

La_2O_3 (99.99%), Tm_2O_3 (99.99%), Eu_2O_3 (99.99%), Er_2O_3 (99.9%), and Yb_2O_3 (99.99%) were purchased from Sinopharm Chemical Reagent Co., Ltd, China, and other chemicals were purchased from Beijing Fine Chemical Company, China. All chemicals are of analytical grade reagents and used as received unless otherwise noted. RE nitrate stock solutions of 0.2 mol/L were prepared by dissolving the corresponding metal oxide in nitric acid at elevated temperature.

Sample preparation

$LaF_3:Yb^{3+}/Er^{3+}$ NCs have been fabricated via a facile hydrothermal route. In a typical experiment, to a 100 mL of beaker containing 20 mL water was added to a water solution (1.5 mL) containing $La(NO_3)_3$, $Yb(NO_3)_3$, and $Er(NO_3)_3$ at a 80:18:2 ratio with a total RE amount of 0.3 mmol. The resulting mixture was thoroughly stirred. Subsequently, an aqueous solution (1.2 mL) containing 1.2 mmol NaF was added and stirred for 30 min. The pH value of the mixture was tuned with sodium hydroxide or nitric acid solution. Subsequently, the solution was transferred to a 40.0 mL Teflon-lined autoclave, and heated at 200 ^oC for 24 h, at which time the mixture was cooled down to room temperature. The resulting nanoparticles were precipitated out through an addition of ethanol, collected by centrifugation, washed with ethanol, and finally dried under 60 ^oC for 12 h. In addition, Eu^{3+} and $Tm^{3+}/Yb^{3+}/Er^{3+}$ doped fluoride were prepared with stoichiometric, and other conditions are the same as those mentioned above for synthesizing $LaF_3:Yb^{3+}/Er^{3+}$ NCs. It should be stated that all samples were hydrothermally treated at 200 °C for 24 h.

Characterization

Powder X-ray diffraction (XRD) data was recorded on a D/Max2550VB+/PC X-ray diffraction meter at a scanning rate of 15°/min in the 2θ range from 15° to 75°, with Cu Ka (40 kV, 40 mA) irradiation (λ=0.15406 nm). Low-resolution and high-resolution transmission electron microscopy (TEM) measurements were carried out on a JEOL 2100 TEM operated at an acceleration voltage of 200 kV. Scanning electron microscopy (SEM) micrographs were obtained using a Hitachi S-4800 FE-SEM. Fourier transform infrared spectroscopy (FTIR) was carried out on a Brucher EQUINX55 spectrometer using KBr pellets. During the luminescence spectroscopic measurements, a 532 nm Verdi-V10 (Coherent) laser pumped Mira 900-F (Coherent) femtosecond laser (tuning wavelength: 700–1000 nm) and a $YAG:Nd^{3+}$ pulsed laser (SHG: 532 nm, THG: 355 nm, Spectra Physics, Quanta Ray Lab-170) were employed as excitation sources. A SP 2750i monochromator (ACTON, spectral resolution: approximately 0.008 nm) equipped with a PIXIS 100 charge coupled device (CCD, ACTON) and a PD471 photomultiplier tube (PMT, ACTON) were used for luminescence collection and detection. Proper light filters were placed in front of the entrance of the monochromator to block the scattering light. All of measurements were conducted out at room temperature.

Results and discussion

Structure and morphology

In our current system, via facile hydrothermal route in a closed system the as-prepared LaF_3 products with multiform structures and morphologies have been synthesized. Many experimental parameters can influence the growth and crystal structure of LaF_3 NCs. Of course, the final morphology of a crystal is also the result of the cooperation of many parameters, such as hydrothermal temperature and reactive time. We kept hydrothermal temperature and reactive time the same, and emphasized the pH value of mother solution effects in the growth of NCs. Interestingly, two different crystal phases were observed in the process of synthesizing the NCs. Fig. 1 shows the XRD patterns of Yb^{3+}/Er^{3+} co-doped LaF_3 NCs hydrothermally treated 24 h under various pH values tuned by employing NaOH solution. All diffraction peaks shown in Fig. 1 can be indexed easily as pure, hexagonal phase of LaF_3 [space group $P\bar{3}c1$ (JCPDS No. 32-0483)], synthesized at a pH value of less than 12. It is worth pointing out that all the peaks have been apparently broadened and weaken with elevating pH values of solutions as shown in Fig. 1(a), indicating the smaller crystal sizes. When pH value up to 14, all of the reflections could be readily indexed to the hexagonal phaseof $La(OH)_3$ [(space group P63/m (JCPDS No. 36-1481)] in Fig. 1(b).[28]

TEM provides further insight into the morphology and microstructural details of the RE based series of LaF_3

nanostructures. Figs. 2(a)-2(f) show typical images of these RE compound nanoparticles, from which it can be seen that the as-obtained LaF_3 NCs at low pH value present the irregularly shape [Fig. 2(a)]. However, the morphology and size of LaF_3 crystallites obtained varied greatly depending upon the pH value of the mother solution. The size of the LaF_3 nanoparicles shrinks from approximately 80 to 20 nm when the pH values of solutions increased from 2 to 12 [Figs. 2(a) and 2(b)], which is in consistent with the analysis of the XRD. Interestingly, when the pH value is adjusted to 12 by employing 5 mol/L NaOH solution, unique and regular hollow-hexagonal shape nanoplates, known as fullerene-like, are yielded in large quantities [Fig. 2(b)]. The high-resolution TEM (HRTEM) image of a single nanosphere provides more detailed structural information on these fullerene-like nanostructures. Fig. 2(c) shows a HRTEM image of LaF_3 nanoparticles with an individual close-caged particle and an approximately 25 nm of outer diameters and 15 nm of inner diameters have been provided as further evidence for the formation of RE fluoride fullerene-like nanostructures. As disclosed by the corresponding HRTEM image, cavities of nanoparticles are half-penetrated, which is confirmed by the lattice stripes within the cavity, as shown in Fig. 2(c). The HRTEM image of a single nanosphere [Fig. 2(c)], indicating that the distance between the adjacent lattice planes is 0.32 nm, is ascribed to (111) crystal plane of the hexagonal phase LaF_3. The corresponding selected area electron diffraction pattern in Fig. 2(d) indicates that the LaF_3 hollow nanospheres are single crystals and the most distinct five concentric diffraction rings can be indexed to (002), (111), (300), (302), (411) and (330) planes from the center, sequentially. When the pH value is further adjusted to 14 by employing NaOH, $La(OH)_3$ microrods with the length and diameter of about 20 μm and 1 μm, respectively, were obtained in Fig. 2(e). No evident modifications on morphology and phase of fluoride products by doping different RE ions are observed. For example, the morphology and phase of Eu^{3+} (2 %) doped fullerene-like LaF_3 nanoparticles prepared at the same conditions of pH are similar as Yb^{3+}/Er^{3+} (18/2 %) doped fullerene-like LaF_3 nanoparticles.

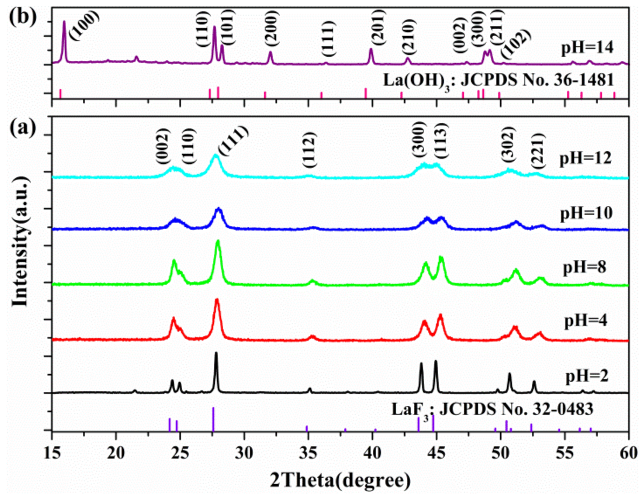

Fig. 1 XRD patterns of LaF_3:Yb^{3+}/Er^{3+} (18/2 %) and $La(OH)_3$:Yb^{3+}/Er^{3+} (18/2 %) samples prepared at different pH values adjusted with NaOH after 24 h at 200 °C and the standard data of hexagonal LaF_3 (JCPDS No. 16-0334) and $La(OH)_3$ (JCPDS No. 36-1481) as references.

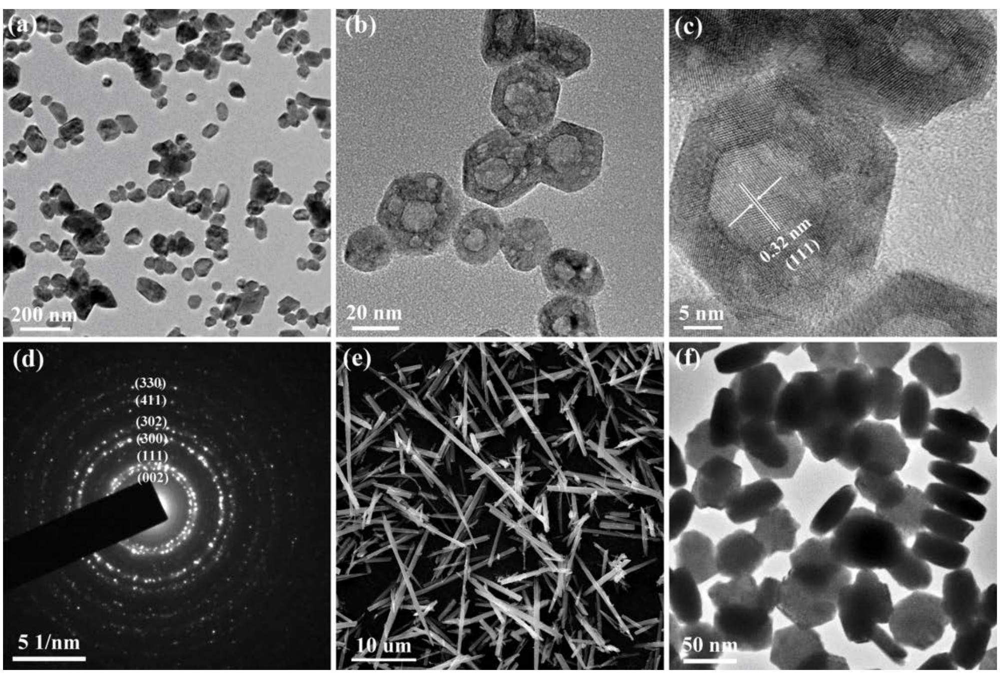

Fig. 2 The influence of the pH values on the shapes of LaF_3:Yb^{3+}/Er^{3+} (18/2 %) NCs at the different pH values adjusted with 5 mol/L NaOH in (a)-(e). (a) Irregular structure obtained at pH=4; (b) and (c) hexagonal nanoplates with hollow structure obtained at pH=12; (d) Selected area electron diffraction pattern corresponding to figure 2(b); (e) Microrods of $La(OH)_3$:Yb^{3+}/Er^{3+} (18/2 %) at a pH=14; (f) Hexagonal nanoplates of LaF_3:Yb^{3+}/Er^{3+} (18/2 %) at a pH of 12 adjusted with ammonia solution (25%). These samples were hydrothermally treated at 200 °C for 24 h.

The strong dependence of morphology and phase on basicity is found in the hydrothermal synthesis of LaF_3 NCs. The weak base like $NH_3.H_2O$ gives the different results, and only LaF_3 NCs are obtained, while $La(OH)_3$ can not be observed at a pH range from 2 to 12. If pH value is tuned to 12 by employing ammonia water, the final product was found to be unique and regular LaF_3

hexagonal plates with an average edge length of about 50 nm and a thickness of 20 nm, as shown in Fig. 2(f). It can be seen from Fig. 2(f) that most of the nanoplates lie flat on the faces, and some stand on their edges. These nanoplates exhibited a relatively narrow size distribution although the edge lengths of the nanoplates shown in the TEM images seemed not very uniform due to the NCs being tilted by different angles on the carbon grid, which is consistent with the previously reported by Chen *et al.*.[29] Similar size-control phenomena for LaF_3 samples have also been observed by employing ammonia water to tune the pH of mother liquid. These results indicate that the control of size, shape and crystal phase of fluoride crystals not only depend on the pH of the initial solution, but also depend on the basicity of the base. A small hydrolysis constant of the alkali would benefit the combination of F^- and RE^{3+} ions to transform RE^{3+} complex into REF_3 lattice.

When different pH values are tuned by using the different basicities, OH^- ligands can capture or release La^{3+} to form $La(OH)_3$ or LaF_3 nucleus, and change ion mobility, solubility as well as density of charges on the growing crystal faces to affect the morphology significantly.[30] As far as the $La(OH)_3$ colloidal precipitates are concerned, the optimal conditions for the formation of $La(OH)_3$ seeds are a basic environment. While the rod or tube shape is common for $La(OH)_3$ crystals with hexagonal layer structures.[31]

The mechanism of the formation of fullerene-like nanoparticles

The influence of chemical potential on the morphology evolution of NCs has been elucidated by Peng *et al*. and in the case of nanostructure with preferential growth direction it would be advantageous to have a higher chemical potential,[32,33] which is mainly determined by the pH value and monomer concentration of the solutions in our reaction system.[34] While small particle size requires high supersaturation,[35] it is expected that, in this case, high supersaturation is achieved by high pH value.

To investigate the growth mechanisms of the fullerene-like LaF_3 nanoparticles, detailed time-dependent experiments were carried out at hydrothermal conditions. The XRD patterns and the corresponding SEM of the intermediates of Yb^{3+}/Er^{3+} co-doped LaF_3 NCs prepared under a pH value of 12 using NaOH solution at different reaction time intervals are shown in Fig. 3 and Fig. 4, respectively. It is clear that after 0.5 h the XRD pattern matches the hexagonal phase of $La(OH)_3$ NCs (space group P63/m, JCPDS No. 36-1481), which is a precursor in the production of LaF_3 NCs. As shown in Fig. 4(a), the diameter and the length of $La(OH)_3$ NCs are about 8 nm and 16 nm, respectively. The hexagonal phase $La(OH)_3$ NCs present preferred growth direction along the c axis. With reaction time prolonging to 5 h, XRD displays a mixed phase composed of hexagonal phase $La(OH)_3$ and hexagonal phase LaF_3 [Fig. 3(b)]. This indicated that the samples transformed partially from hexagonal phase $La(OH)_3$ to hexagonal phase LaF_3. Evidence can also be seen from the TEM image in Fig. 4(b). Here we can see that the new hexagonal nanoplates with a size of ~20 nm and some nanorods disappeared. Based on the above analysis of XRD, it can be appointed that the hexagonal nanoplates of hexagonal LaF_3 phase is formed, as disappears the nanorods of hexagonal $La(OH)_3$ phase. The changes on the phase, morphology and size from Fig. 4(a) to 4(b) indicate that the products undergo a dissolve-renucleation process. This is different from the course of evolution of hexagonal $NaYF_4$ NCs obtained from commercial Y_2O_3 by in-situ ion exchange process without the changes on the size and morphology.[36] When the time is further increased to 12 h, pure hexagonal phase (JCPDS No. 32-0483) [Fig. 3(c)] and the desired hexagonal solid nanoplates without hollow structure [Fig. 4(c)] can be obtained. Extending the thermally treating time to 24 h, hexagonal phase hollow LaF_3 plates with diameters of 25 nm can be easily obtained [Fig. 3(d) and Fig. 4(d)].

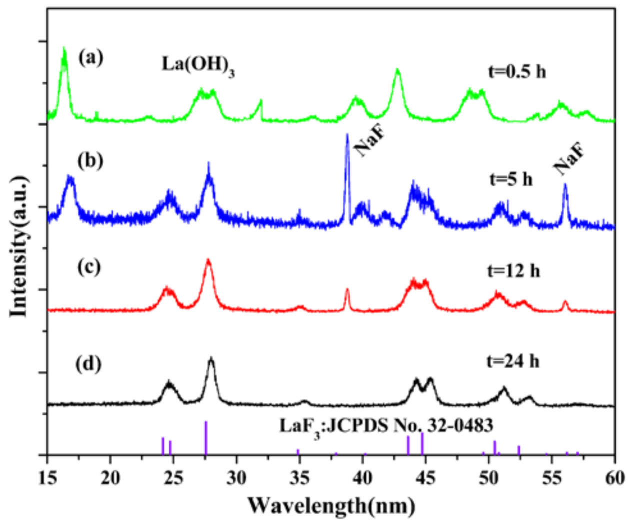

Fig. 3 XRD images of LaF_3:Yb^{3+}/Er^{3+} (18/2 %) samples obtained under a pH value of 12 collected at different reactive time of 0.5 h (a), 5 h (b), 12 h (c) and (d) 24 h.

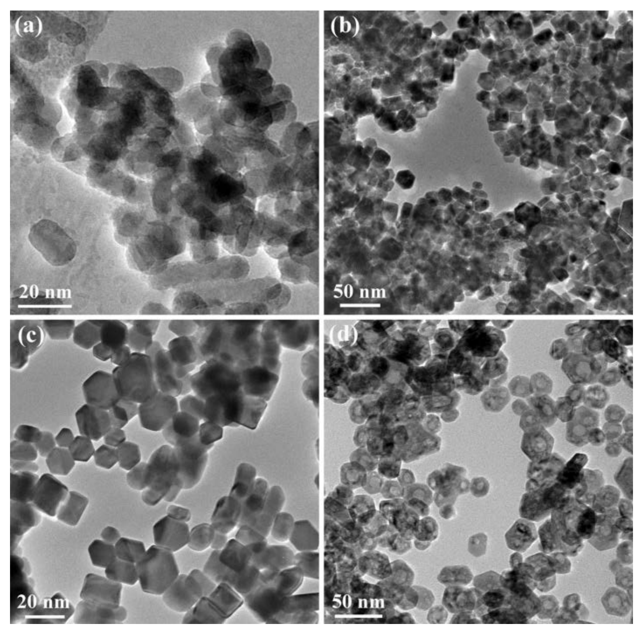

Fig. 4 TEM images of LaF_3:Yb^{3+}/Er^{3+} (18/2 %) samples obtained under a pH value of 12 collected at 0.5 h (a), 5 h (b), 12 h (c) and (d) 24 h.

Based on the time-controlled experiment, the specfic mechanism of morphology control of LaF_3 NCs can now be further addressed as depicted in Scheme 1. Under the low pH value, many primary LaF_3 monomers aggregate to particle without preferential growth orientation resulting in an irregular shape under hydrothermal conditions. The formation of the NCs follows the aggregation growth theory at a pH range from 2 to 10. This mechanism requires that a sufficient amount of ions and primary particles participate in the growth process in order to obtain an aggregation growth. When the pH was adjusted between 11 and 12, it is easier to form mono- and poly-nuclear $La(OH)_3$ species or $La(H_2O)_x$ species accompanied with NaF species, serving as the nucleate seeds in precursor solution at room temperature. When the mixture solution was transferred to an autoclave, the nucleate seeds further crystallize and coarsen. However, as heating up to a certain temperature, the $La(OH)_3$ species seem not to be the stable phase. It is reported that the NaF monomer also was the quasi-steady state species and its molar ratios over the other fluorides were the key factors to decide the growth rate and the sizes of final $NaYF_4$ particles.[6] With the hydrothermal process evolving, the energy provided by the reaction system becomes higher until a certain moment when it is high enough to overcome the reaction energy barrier. The $La(OH)_3$ solid nanospheres become dissolved through a dissolution-recrystallisation process and the LaF_3 nanoflosses are formed which are adsorbed on the larger $La(OH)_3$ solid nanospheres (step 3 in Scheme 1) because the hexagonal phase LaF_3 is a thermodynamically more stable structure. The growth modes are different from the tubular hexagonal $NaYF_4$ NCs by fluorinating an RE–OH bond to RE–F bond fluoride.[37] The transformation process can be described with the following equations.

$2La(OH)_3+7NaF \rightarrow LaF_3+NaLaF_4+6Na^++6OH^-$;

$3NaLaF_4+ La^{3+} \rightarrow 4LaF_3+3Na^+$.

During the further growth process of LaF_3 crystals, $RE(OH)_3$ monomers in solution fast redissolved under the hydrothermal conditions and RE^{3+} ions diffuse onto the surface of a growing crystal and their subsequent fast incorporation with F^- into the LaF_3 lattice. While generated OH^-, that is the weak capping ligand, is preferentially bound to the highest-energy {0001} surfaces of LaF_3 (Scheme 1), which suppresses the growth of nuclei along {0001} surfaces. The growth of LaF_3 along six symmetric directions of {1010} finally results in hexagonal plate particles at a pH of 12.

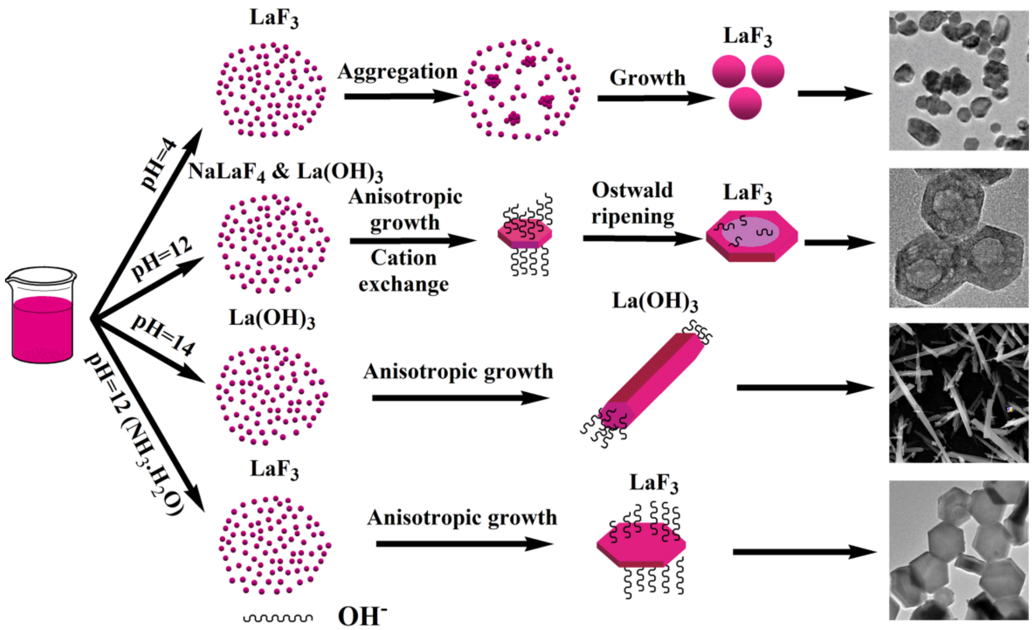

Scheme 1 Schematic illustration for the possible formation processes of β-LaF_3:Yb^{3+}/Er^{3+} (18/2 %) and $La(OH)_3$:Yb^{3+}/Er^{3+} (18/2 %) NCs with various morphologies using NaF as fluoride at different pH values.

This feeding mode can be regarded as a similar process to the "injection single precursor" technique,[38] which will ensure a higher monomer concentration of LaF_3 by the redissolved $La(OH)_3$ and NaF species. $La(OH)_3$ and NaF species therefore seem to act as a homogeneously dispersed reservoir of monomers.[39] If $La(OH)_3$ and NaF species as a reservoir releases monomers at a rate sufficient to ensure a moderate to high level of supersaturation during the first stage of the LaF_3 particles growth, focusing of sizes by diffusion-control will occur in accord with the observed narrow particle size distribution and regular hexagonal plate of final products.[8,40] In this stage, the LaF_3 particles grow very fast, while the molar fraction of precursor $La(OH)_3$ particles as the provider of monomers rapidly decrease. As long as $La(OH)_3$ molar fraction is not too low, a few of $RE(OH)_3$ crystal seeds inevitably growth at a higher monomer concentration solution due to the phase matching between LaF_3 and $La(OH)_3$.

However, LaF_3 solid solution particles containing impurities phase such as $La(OH)_3$ and $NaLaF_4$ are weak crystalline due to a rapid grow rate in the first region. In the subsequent stage, most of the $La(OH)_3$ particles have already been consumed and the growth rate of the LaF_3 particles controlled by the diffusion rate of monomers will present downward trend. Since $La(OH)_3$ crystals is thermodynamically less stable than LaF_3, $La(OH)_3$ particles finally are depleted. The inner crystallites of this LaF_3 hexagonal plate might be weaker than that of outer owing to the decline in grow rate, which make the inner weak crystallites dissolve and transfer out by a localized Ostwald ripening and the cation exchange between La^{3+} and Na^{+}.[12] Faster ionic motion usually ensures a reversible pathway between the fluid phase and the solid phase, which allows atoms, ions, or molecules to adopt correct positions.[41] Matter relocation during prolonged processes, which is indispensable in the ripening, may also result in unexpected hollow structure if starting solid precursors become compositionally complicated.

When the pH up to 14 employing NaOH, a higher pH implies a higher OH^- ion concentration and a higher chemical potential in solution. A higher chemical potential is preferable for the growth of nanowires. However, higher OH^- ion concentrations result in a higher concentration of $La(OH)_3$ monomers and thus reduce the rate of ionic motion. Finally, few LaF_3 seeds were obtained due to exhaustion of La^{3+} ions. In following hydrothermal process, dissolution of $La(OH)_3$ monomers is restricted by the value of K_{sp} for $La(OH)_3$. Therefore, $La(OH)_3$ microrods, instead of LaF_3 particles, is formed similar to previous reports by Wang *et al*..[34]

When ammonia water is employed to adjust pH value of solution, LaF_3 precipitate is prior to form due to the low value of dissociation constant for $NH_3.H_2O$, which leads to form LaF_3 crystals. When further elevating pH, unique and regular hexagonal plates are obtained because OH^- ligand preferentially bound to the highest-energy {0001} surfaces of growing crystal.[12] So these results proved employing strong base to adjust the pH value of solutions was necessary to form the hollow hexagonal plates, which will allow the formation of intermediate $RE(OH)_3$ and result in a complicated primary particles. Scheme 1 depicts a proposed schematic illustration of the nucleation and growth processes of the NCs. The irregular sphere formation can be explained by the aggregated particles accompanied, while the formation of a hexagonal hollow nanodisc crystal can be ascribed to the localized Ostwald ripening and a cation exchange mechanism.[25,26,42] In our experiment, OH^- ions play an important role in the process. OH^- not only can promote the growth along six symmetric directions by adsorbing on {0001} planes, but also promote the localized Ostwald ripening by introduction of impurity phase of $La(OH)_3$.

The photoluminescence properties of doped fullerene-like LaF_3 nanoparticles

The UC luminescence of RE ions has been investigated extensively because of their potential application in various fields, i.e. lighting or display, IR detection and medical imaging.[43–46] RE fluorides with a high refractive index and low phonon energy, have become a research focus on the materials field owing to their unique applications based on optical characteristics arising from the 4f electrons. To examine the feasibility of the as-obtained NCs as efficient UC host materials, the most frequently used UC ion Er^{3+} and the sensitizer ion Yb^{3+} were co-doped into a series of LaF_3 samples synthesized under the different pH value conditions. Fig. 5 shows UC emission spectra of a series of Yb^{3+}/Er^{3+} co-doped LaF_3 samples in the range of 500–700 nm under 980 nm excitation. All transitions are signed to the Er^{3+} ion. Green luminescence corresponding to the $^2H_{11/2}/^4S_{3/2}\rightarrow{}^4I_{15/2}$ transitions locates in the wavelength region of 500–575 nm, and the $^4F_{9/2}\rightarrow{}^4I_{15/2}$ transition derived red luminescence ranges from 625 to 700 nm. The weak emission at about 410 nm is attributed to $^2H_{9/2}–^4I_{15/2}$ transition. These UC peaks in Fig. 5 is in agreement with what have been reported for Yb^{3+}/Er^{3+} UC in $NaYF_4$ NCs.[47–50] It is noticed that the luminescence emission intensity and the ratio of red to green emission bands in Yb^{3+}/Er^{3+} codoped LaF_3 can be tuned by adjusting the pH value of mother liquids. Obviously, the Er^{3+} and Yb^{3+} double-doped LaF_3 NCs display the strong UC emission, and even the white light can be observed by naked eye when $Yb^{3+}/Tm^{3+}/Er^{3+}$ are co-doped in LaF_3 NCs. These spectra measurements indicate LaF_3 host synthesized by hydrothermal route is a kind of efficient UC host materials.

In addition to, it is noticed that the luminescence emission intensity and the ratio of red to green emission bands in Yb^{3+}/Er^{3+} double-doped LaF_3 NCs can be tuned by adjusting the pH values of mother liquids. As shown in Fig. 5, the UC luminescence emission of Yb^{3+}/Er^{3+} codoped LaF_3 synthesized under acid condition present the stronger luminescence intensity and the lower ratio of red to green emission bands than that of Yb^{3+}/Er^{3+} double-doped LaF_3 synthesized under basic environment.

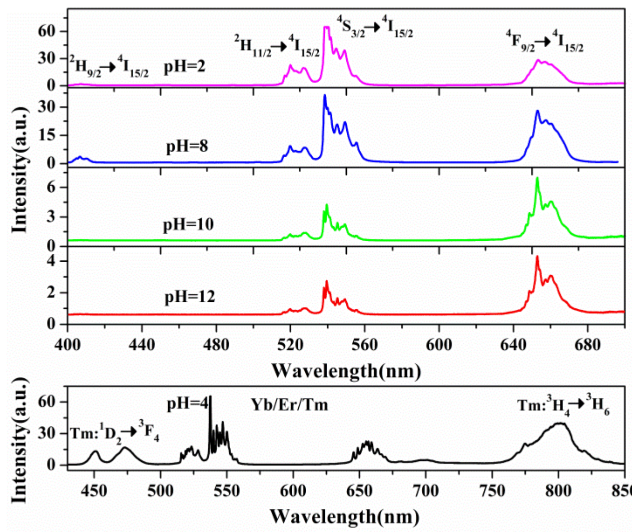

Fig. 5 UC luminescence spectra of LaF_3:Yb^{3+}/Er^{3+} (18/2 %) NCs prepared at pH=2, 8, 10 and 12, and LaF_3:$Yb^{3+}/Tm^{3+}/Er^{3+}$ (18/1/2 %) NCs prepared at pH=4 under continuous-wave laser excitation at 980 nm (power ≈ 600 mW).

Our recent reports show that the luminescence intensity depends on quality of crystallization, particle size, crystallographic phase, composition of host matrix and even local symmetry of matrix.[51, 52] In order to verify the influence of local environment symmetry on luminescence intensity, the photoluminescence spectra of a series of Eu^{3+} doped LaF_3 prepared under different pH values are carried out shown in Fig. 6. The spectra are characteristic of the $^5D_1\rightarrow{}^7F_0$ and $^5D_0\rightarrow{}^7F_j$ line emissions (J=0, 1, 2, 3, 4) of the Eu^{3+} ion.[53, 54] Interestingly, we noted that the total intensity of luminescence became weaker (Fig. 6), while the relative intensity ratio of $^5D_0\rightarrow{}^7F_2$ to $^5D_0\rightarrow{}^7F_1$ transition became stronger with an increase of the value of pH (Fig. 6), and the ratio of I_{615}/I_{590} for (a)-(d) in Fig. 6 are 0.71, 0.72, 0.90 and 1.29, respectively. It is well-known that the $^5D_0\rightarrow{}^7F_2$ transition is electric-dipole transition, and its intensity is significantly affected by the symmetry in local environments around Eu^{3+} ions. When the symmetry around the Eu^{3+} ions is lowered, the transition probability of the $^5D_0\rightarrow{}^7F_2$ is increased. However, the $^5D_0\rightarrow{}^7F_1$ transition is magnetic-dipole allowed and is relatively insensitive to the local symmetry.[55] Thus, the symmetry around the Eu^{3+} ions decreased when increasing the value of the pH, which indicates that the crystal field surrounding the Eu^{3+} ions is affected by the decrease of size and hollow fullerene-like structure. But the symmetry around the Eu^{3+} ions induced by the small size of particles with the fullerence structure can not result in a decrease on luminescence. The reduction in emission intensity in the fullerence nanoplates with the hollow structure is caused by the adsorption of a great amount of OH^-, on the surface and the hollow structure. Stretching from OH^- groups and CO_3^{2-} yields high energy vibrations (3350 and 1550 cm^{-1}, respectively) that can increase the multi-phonon relaxation rate of the metastable states and thus reduce the overall visible emission intensity and lower ratio of the green-to-red emission.[56,57] This is supported by FTIR of $LaF_3:Eu^{3+}$ samples prepared at different pH conditions as shown in Fig. 7, in which the FTIR spectra intensity of OH^- and CO_3^{2-} sharply increase with pH elevating.

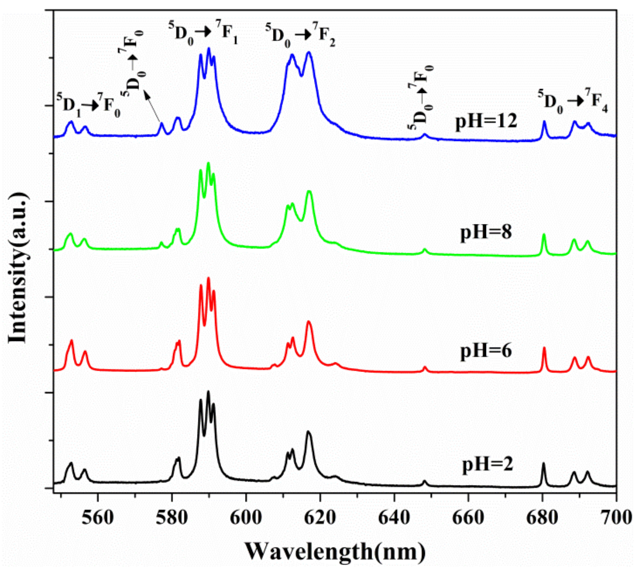

Fig. 6 Luminescence emission spectra of $LaF_3:Eu^{3+}$ (2 %) samples with 532 nm excitation prepared at pH=2, 6, 8 and 12, respectively. The spectra were normalized to 590 nm emissions.

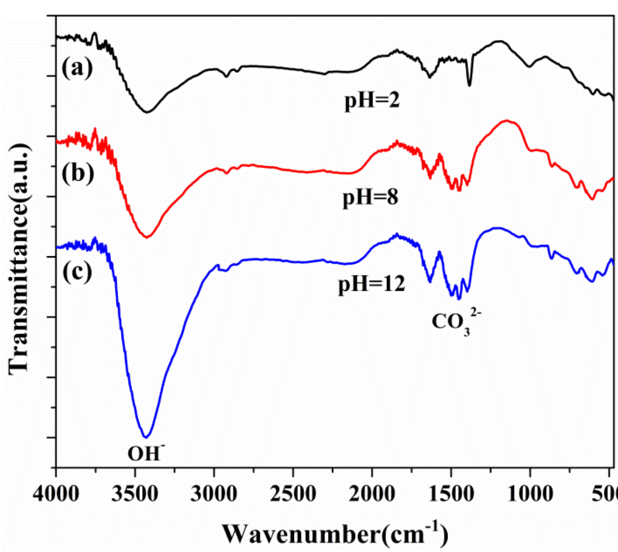

Fig. 7 FTIR of $LaF_3:Eu^{3+}$ (2 %) samples prepared at different pH conditions. (a) pH=2, (b) pH=8, and (c) pH=12.

As is well-known, the UC intensity and the ratio of red to green depend on the population of the intermediate states. The UC mechanism in Er^{3+} and Yb^{3+} codoped systems is well known and occurs via two successive transfers of energy from the Yb^{3+} ion to the Er^{3+} ion. Following 980 nm irradiation, firstly, Er^{3+} ions in the $^4I_{15/2}$ state are excited to $^4I_{11/2}$ state via energy transfer between Yb^{3+} and Er^{3+}. Subsequent, the $^4I_{13/2}$ levels are populated by radiative or noradiative relaxations of $^4I_{11/2}\rightarrow{}^4I_{13/2}$. In the second-step excitation, the same laser pumps the excited-state electrons from $^4I_{11/2}$ to $^4F_{7/2}$ levels via energy transfer or from $^4I_{13/2}$ to $^4F_{9/2}$ states via phonon-assisted energy transfer. Subsequent, the $^4S_{3/2}$ state may be populated by nonradiative relaxations of $^4F_{7/2}\rightarrow{}^4S_{3/2}$ in $LaF_3:Yb^{3+}/Er^{3+}$ NCs with low phonon obtained at low pH. In $LaF_3:Yb^{3+}/Er^{3+}$ fullerence nanoplates, with high energy phonon groups including OH^- and CO_3^{2-}, $^4F_{7/2}$ state can effectively relax to red luminescent $^4F_{9/2}$ levels by activating cross-relaxation channels of $^4F_{7/2}+{}^4I_{11/2}\rightarrow{}^4F_{9/2}+{}^4F_{9/2}$ with high energy phonon. As anticipated, the nonradiative cross-relaxations promoted the red emission and reduced the green emission and the total visible emission in $LaF_3:Yb^{3+}/Er^{3+}$ fullerence nanoplates.[58,59] The proposed conversion mechanism of $LaF_3:Yb^{3+}/Er^{3+}$ fullerence nanoplates is shown in Fig. 8. Therefore, $LaF_3:Yb^{3+}/Er^{3+}$ fullerence nanoplates had stronger red emission following near-infrared excitation, which could be used as carrier of targeted drugs for bioapplications. These results indicate that the synthetic method is ideal since it allows tailoring of the UC emission properties of the material simply by varying the pH of mother liquid.

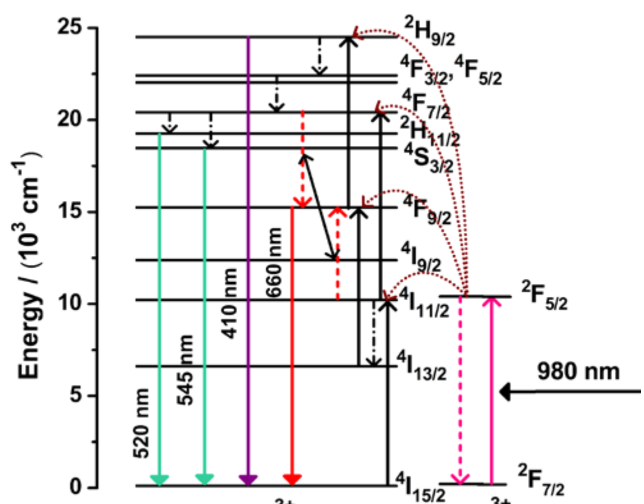

Fig. 8 Schematic of the various upconversion mechanisms in nanocrystalline $LaF_3:Yb^{3+}/Er^{3+}$ (18/2 %) following excitation with 980 nm.

Conclusions

In summary, $LaF_3:Yb^{3+}/Er^{3+}$ NCs including nanoparticles, hexagonal nanoplates as well as fullerene-like nanoplates and $La(OH)_3:Yb^{3+}/Er^{3+}$ microrods have been successfully synthesized via a simple and mild hydrothermal route at designated pH values. It is interesting to observe that the hexagonal nanoplates are hollow structure, known as inorganic fullerene-like nanoparticles. XRD, SEM, TEM, HRTEM and photoluminescence spectra were used to characterize the samples. It is found that the formation of monodispersed fullerene-like LaF_3 NCs not only closely correlates with the pH values of the mother solutions, but also depends on the basicity of the base employed adjusting pH value. The formation mechanism is related to the Ostwald ripening, in which the inner weak crystallites by introduce mixed impurity phase are the crucial step in the formation of the LaF_3 fullerene-like nanostructures. The strong alkaline solution in the absence of any organic additive in this system was found to be a prerequisite for producing hexagonal fullerene-like LaF_3 nanoplates. The interesting luminescence properties are discussed in detail. It is noticed that the luminescence emission intensity and the ratio of red to green emission bands in of Yb^{3+}/Er^{3+} co-doped LaF_3 can be tuned by adjusting pH value of mother liquids, which indicates that the synthetic methods is ideal since it allows tailoring of the UC emission properties of the material simply by varying the pH of mother liquid. The regular fullerene-like hexagon nanoplates with tunable luminescence emission are conducive to serve as novel building blocks for new nanodevice applications.

Acknowledgements

The authors acknowledge the financial support of the Natural Science Foundation of Shaanxi Province of China (Grant No. 2014JQ1008), the Special Foundation of Shaanxi Educational Commission of China (Grant No. 12JK0453), the Talent Fund of Subject Construction (Grant No. DB12065) and Youth Foundation (Grant No. QN1237) of Xi'an University of Architecture and Technology.

Notes and references

[a]*College of Science, Xi'an University of Architecture and Technology, Xi'an, Shaanxi 710055, China. E-mail: gaodangli@163.com*
[b]*Electronic Materials Research Laboratory (EMRL), Key Laboratory of Education Ministry, International Center for Dielectric Research, Xi'an Jiaotong University, Xi'an, Shaanxi 710049, China*
[c]*College of Physics and Information Technology, Shaanxi Normal University, Xi'an, Shaanxi 710062, China.*

1 A. M. Cross, P. S. May, F. C. J. M. van Veggel and M. T. Berry, *J. Phys. Chem. C*, 2010, **114**, 14740.
2 C. Lorbeer and A. V. Mudring, *J. Phys. Chem. C*, 2013, **117**, 12229.
3 X. Wang, J. Zhuang, Q. Peng and Y. D. Li, *Inorg. Chem.*, 2006, **45**, 6661.
4 Y. W. Zhang, X. Sun, R. Si, L. P. You and C. H. Yan, 2005, *J. Am. Chem. Soc.*, **127**, 3260.
5 H. X. Mai, Y. W. Zhang, R. Si, Z. G. Yan, L. D. Sun, L. P. You and C. H. Yan, *J. Am. Chem. Soc.*, 2006, **128**, 6426.
6 G. S. Yi and G. M. Chow, *Adv. Funct. Mater.*, 2006, **16**, 2324.
7 J. C. Boyer, F. Vetrone, L. A. Cuccia and J. A. Capobianco, 2006, *J. Am. Chem. Soc.*, **128**, 7444.
8 B. Voß, J. Nordmann, A. Uhl, R. Komban and M. Haase, *Nanoscale*, 2013, **5**, 806.
9 D. L. Gao, X. Y. Zhang, H. R. Zheng, W. Gao and E. J. He, *J. Alloy Compd.*, 2013, **554**, 395.
10 V. F. Puntes, D. Zanchet, C. K. Erdonmez and A. P. Alivisatos, *J. Am. Chem. Soc.*, 2002, **124**, 12874.
11 M. B. Sigman, A. Ghezelbash, T. Hanrath, A. E. Saunders, F. Lee and B. A. Korgel, *J. Am. Chem. Soc.*, 2003, **125**, 16050.
12 D. L. Gao, W. Gao, P. Shi and L. Li, *RSC Adv.*, 2013, **3**, 14757.
13 D. L. Gao, X. Y. Zhang and W. Gao, *ACS Appl. Mater. Interfaces*, 2013, **5**, 9732.
14 Z. Y. Wang, Z. C. Wang, H. B. Wu and X. W. D. Lou, *Sci. Rep.*, 2013, **3**, 1391.
15 X. Y. Lai, J. E. Halpert and D. Wang, *Energy Environ. Sci.*, 2012, **5**, 5604.
16 Z. M. Chen, Z. R. Geng, M. L. Shi, Z. H. Liu and Z. L. Wang, *Langmuir*, 2010, **26**, 14271.
17 H. H. Gorris and O. S. Wolfbeis, *Angew. Chem. Int. Ed.*, 2013, **52**, 3584.
18 Z. Wang, L. Wu, M. Chen and S. Zhou, *J. Am. Chem. Soc.*, 2009, **131**, 11276.
19 F. Wang and X. G. Liu, *Chem. Soc. Rev.*, 2009, **38**, 976.
20 M. Chen, L. Xie, F. Y. Li, S. X. Zhou and L. M. Wu, *ACS Appl. Mater. Interfaces*, 2010, **2**, 2733.
21 J. N. Shan, N. Yao, Y. G. Ju, *J. Nanopart. Res.*, 2010, **12**, 1429.
22 G. Jia, Y. H. Song, H. P. You and H. J. Zhang, *Cryst. Growth Des.*, 2009, **1**, 301.
23 F. Zhang, Y. F. Shi, X. H. Sun, D. Y. Zhao and G. D. Stucky, *Chem. Mater.*, 2009, **21**, 5237.
24 J. Hu, M. Chen, X. S. Fang and L. M. Wu, *Chem. Soc. Rev.*, 2011, **40**, 5472.
25 Z. M. Chen, Z. R. Geng, M. L. Shi, Z. H. Liu and Z. L. Wang, *CrystEngComm*, 2009, **11**, 1591.
26 Z. M. Chen, Z. R. Geng, Z. Y. Zhang, Z. H. Liu and Z. L. Wang, *CrystEngComm*, 2010, **12**, 2841.
27 L. Ma, W. X. Chen, Y. F. Zheng, J. Zhao and Z. D. Xu, *Mater. Lett.*, 2007, **61**, 2765.
28 X. Zhang, P. P. Yang, D. Wang, J. Xu, C. X. Li, S. L. Gai and J. Lin, *Cryst. Growth Des.*, 2012, **12**, 306.
29 C. H. Liu and D. P. Chen, *J. Mater. Chem.*, 2007, **17**, 3875.
30 Z. G. Yan and C. H. Yan, *J. Mater. Chem.*, 2008, **18**, 5046.
31 X. Wang and Y. D. Li, *Chem. Eur. J.*, 2003, **9**, 5627.
32 Z. A. Peng and X. G. Peng, *J. Am. Chem. Soc.*, 2001, **123**, 1389.
33 Z. A. Peng and X. G. Peng, *J. Am. Chem. Soc.*, 2002, **124**, 3343.
34 X. Wang and Y. D. Li, *Angew. Chem. Int. Ed.*, 2002, **41**, 4790.
35 Y. J. Sun, Y. Chen, L. J. Tian, Y. Yu, X. G. Kong, J. W. Zhao and H. Zhang, *Nanotechnology*, 2007, **18**, 275609.
36 J. L. Zhuang, J. Wang, X. F. Yang, I. D. Williams, W. Zhang, Q. Y. Zhang, Z. M. Feng, Z. M. Yang, C. L. Liang, M. M. Wu, and Q. Su, *Chem. Mater.*, 2009, **21**, 160.
37 F. Zhang and D. Y. Zhao, *ACS Nano*, 2009, **3**, 159.
38 X. Liang, X. Wang, J. Zhuang, Q. Peng and Y. D. Li, *Adv. Funct. Mater.*, 2007, **17**, 2757.
39 T. Sugimoto, *Adv. Colloid Interface Sci.*, 1987, **28**, 65.
40 M. D. Clark, S. K. Kumar, J. S. Owen, E. M. Chan, *Nano Lett.*, 2011, **11**, 1976.
41 T. J. Trentler, K. M. Hickman, S. C. Goel, A. M. Viano, P. C. Gibbons and W. E. Buhro, *Science*, 1995, **270**, 1791.
42 Y. Cheng, Y. S. Wang, D. Q. Chen and F. Bao, *J. Phys. Chem. B*, 2005, **109**, 794.
43 Y. Wang, L. Ji, B. B. Zhang, P. H. Yin, Y. Y. Qiu, D. Q. Song, J. Y. Zhou and Q. Li, *Nanotechnology*, 2013, **24**, 175101.
44 Z. M. Yang, Z. M. Feng and Z. H. Jiang, 2005, *J. Phys. D: Appl. Phys.*, **38**, 1629.
45 R. Calderón-Villajos, C. Zaldo and C. Cascales, *Nanotechnology*, 2012, **23**, 505205.
46 V. K. A. Sreenivasan, A. V. Zvyagin and E. M. Goldys, *J. Phys.: Condens. Matter*, 2013, **25**, 194101.
47 F. Wang and X. G. Liu, *J. Am. Chem. Soc.*, 2008, **130**, 5642.
48 F. Wang, Y. Han, C. S. Lim, Y. H. Lu, J. Wang, J. Xu, H. Y. Chen, C. Zhang, M. H. Hong and X. G. Liu, *Nature*, 2010, **463**, 1061.
49 J. Shen, G. Chen, T. Y. Ohulchanskyy, S. J. Kesseli, S. Buchholz, Z. Li, P. N. Prasad and G. Han, *Small*, 2013, **9**, 3213.
50 S. Georgescu, A. M. Voiculescu, C. Matei, C. E. Secu, R. F. Negrea and M. Secu, *J. Lumin.*, 2013, **143**, 150.
51 D. L. Gao, X. Y. Zhang and W. Gao, *J. Appl. Phys.*, 2012, **111**, 033505.
52 D. L. Gao, H. R. Zheng, X. Y. Zhang, W. Gao, Y. Tian, J. Li and M. Cui, 2011, *Nanotechnology*, **22**, 175702.
53 J. W. Stouwdam and F. C. J. M. van Veggel, *Nano Lett.*, 2002, **2,** 733.
54 D. L. Gao, H. R. Zheng, X. Y. Zhang, Z. X. Fu, Z. L. Zhang, Y. Tian and M. Cui, *Appl. Phys. Lett.*, 2011, **98**, 011907.

55 D. Lin-Vien, N. B. Colthup, W. G. Fateley and J. G. Graselli, *The Hand-book of IR and Raman Characteristic Frequencies of Organic Molecules*, (New York: Academic) 1991.
56 J. X. Fu, X. H. Fu, C. M. Wang, X. F. Yang, J. L. Zhuang, G. G. Zhang, B. Y. Lai, M. M. Wu and J. Wang, *Eur. J. Inorg. Chem.*, 2013, **2013**, 1269.
57 Z. G. Xia and P. Du, *J. Mater. Res.*, 2010, **25**, 2035.
58 F. Vetrone, J. C. Boyer, J. A. Capobianco, A. Speghini and M. Bettinelli, *J. Appl. Phys.*, 2004, **96**, 661.
59 J. W. Zhao, Y. J. Sun, X. G. Kong, L. J. Tian, Y. Wang, L. P. Tu, J. L. Zhao and H. Zhang, *J. Phys. Chem. B*, 2008, **112**, 15666.

Graphical Abstract

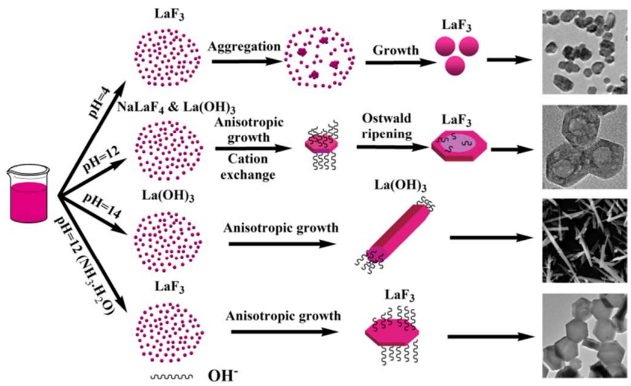

The formation of fluoride NCs closely correlates with the pH and the basicity of the base employed adjusting pH.